X- and C-Band SAR Data to Monitoring Ground Deformations and Slow-moving Landslides for the 2016 Manta and Portoviejo Earthquake (Manabì, Ecuador)

Diego Di Martire*, Pierluigi Confuorto*, Annalisa Frezza* Massimo Ramondini*
{diego.dimartire, pierluigi.confuorto, ramondin}@unina.it,
frezza.annalisa@libero.it

A. Vàzquez Lòpez†
alfredo.vazquez@ucuenca.edu.ec

Maria Pia Del Rosso‡, Alessandro Sebastianelli‡, Silvia L. Ullo‡
mariapia.delrosso@gmail.com, alessandroseba1995@gmail.com, ullo@unisannio.it

* University Federico II of Naples, Italy
† University of Cuenca, Ecuador
‡ University of Sannio, Benevento, Italy

***Abstract*—Ground deformation due to catastrophic natural events have a powerful destructive potential both on people and buildings. In recent years Remote Sensing techniques have proved to be very useful to detect and monitor earth surface and ground deformation phenomena, by helping with their a priori and a posteriori analysis. In particular, Differential SAR Interferometry is widely implemented for such scenarios. In this work, such technique has been applied to observe the effects of the 7.8 Mw earthquake that hit the coast of Ecuador on April 16, 2016. Displacement maps were generated from Sentinel-1 data and compared with the damage reported in the city of Portoviejo, highlighting several critical situations and showing very interesting results. The paper allows to underline the usefulness of using Differential SAR Interferometry and Remote Sensing together with ground truth data comparison. The results so far obtained provide a first base for further evaluations, by using also COSMO-SkyMed imagery, which will represent a valid support for land management authorities.**

***Index terms*—** Differential SAR Interferometry, Earthquake, Monitoring, COSMO-SkyMed, Sentinel-1, damage evaluation.

I. Introduction

Ground deformation phenomena, either of natural and man-made origin, are widespread in the entire world and are one of the primary cause for economic and social losses. They have sensibly increased, and recent trend forecast even more losses in the future [1]. Among the most cata-strophic natural events, earthquakes are worth to be mentioned as the most disruptive, causing direct damage to people and building, and also triggering other natural hazards, such as landslides. Monitoring of ground displacements is fundamental and represents a primary goal for scientists and stakeholders responsible for land management, aiming at the reduction and the forecasting of such events. Spaceborne remote sensing has provided a full support due to their capacity of observing wide areas in a relatively short amount of time. For instance, Differential Synthetic Aperture Radar Interferometry (DInSAR) is a worthwhile device widely implemented for the detection and the monitoring of ground deformation phenomena (e.g. earthquakes [2] [3], subsidence [4] [5], landslides [6] [7]) with an extreme accuracy, especially since the launch of the modern space-borne constellations (TerraSAR-X, COSMO-SkyMed and Sentinel-1), characterized by resolution up to 3m and revisit time of the orbit up to 4 days. Here, SAR interferometry has been applied to observe the effects of the 7.8 Mw earthquake that struck along the central coast of Ecuador on April 16, 2016, causing 688 victims and extensively damaging the provinces of Esmeralda and Manabì. DInSAR analyses were here focused on the city of Portoviejo, the capital of the Manabì province, where more than 500 civilian building and main infrastructures, sometimes necessary for the economy of the city, collapsed in the aftermath of the seismic movement, as well as several landslides were activated or re-activated, due to liquefaction or to additional pore water dissipation. Two different datasets and two different techniques were implemented. On one hand, Sentinel-1 data, acquired before $(03/04/2016)$ and after the main shock of April 2016 $(27/04/2016)$ were processed by means of Sentinel Application Platform (SNAP) toolbox, an open source software by European Space Agency (ESA) to obtain displacement maps useful to analyze and quantify the effects of the shake on the surface and on the main civilian structures of the city. In addition, a first result obtained by using a Persistent Scatterer approach (PS), the Coherent Pixel Technique [8], on COSMO-SkyMed imagery is provided, hence introducing the future perspective of this work. The results have been thus critically analyzed, pointing out the role of DInSAR as a valuable tool for the detection and the analysis of ground deformation phenomena, providing a complete support for land management authorities. The paper is organized as follows: in the next Section some information is given on the earthquake that hit the coast of Ecuador on April 16, 2016 and an analysis of its geological situation is presented. In Section III the technique used to observe the effects of the earthquake is explained, and satellite data used at this end are discussed with their main characteristics. Results are shown in Section IV and Section V highlights conclusions and future work.

II. EARTHQUAKE AND GEOLOGICAL SETTING

On April 16, 2016, the central coast of Ecuador was hit by an earthquake with a moment magnitude (Mw) equals to 7.8, whose epicenter was located south of Muisne and north of Manta and Portoviejo [9], and hypocenter at depth of 19.2 km, causing widespread damage on several cities located along the coast (Fig. 1). The earthquake may be attributed to the

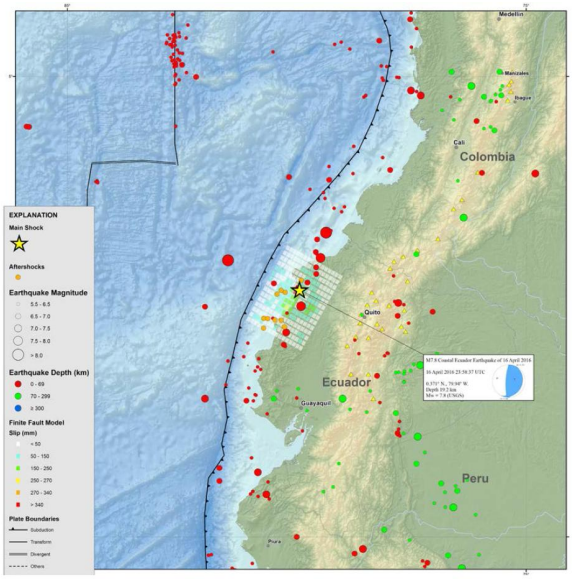

Figure 1: Regional seismicity of Ecuador, with a focus on 7.8 Mw event occured in 2016 (courtesy of USGS, 2016)

dynamic of a megathrust at the boundary on the Nazca Plate, subducting beneath the South America Plate, with a displacement rate of approximately 61 mm/yr [9]. Following the main shock, there had been more than 2.000 aftershocks [10], with three in the specific, characterized by a moment magnitude higher than 6 [11]. Ecuador seismic history is strictly related to the subduction zone, whereas seven magnitude 7 or even greater earthquakes have occurred within the range of 250 km of the April 16, 2016 event, since 1900 [9]. These earthquakes, including the 2016 sequence, are thus all related to the interface seismicity of the northern central section of the Ecuadorian subduction, peculiar for the greater dip angles (16 to 25°) and larger recorded magnitudes associated to shallower interface events than the southern section of the subduction, dipping at an angle of 10° and whose seismicity is governed mostly by in-slab events [12] [13]. The distribution of the seismicity of the area, moreover, may be explained by the presence of the Carnegie Ridge [14] [15] [16]. Ground motion records are provided by the Ecuadorian Physical Institute [17], which observed, through accelerographic data, peak ground acceleration lower in the northern part (Esmeraldas and San Lorenzo stations) while greater peak acceleration values were obtained at south (Portoviejo, Manta and Chone, 0.38, 0.52 and 0.37 g, respectively) [17], which explained also the higher damage rate in this part of the earthquake-affected area. This might be due to the geological configuration of the terrains of the above-mentioned cities. In particular, the city object of the present study, Portoviejo, is characterized by the presence of alluvial deposits and terraces (with thickness of 10 and 40 m respectively and Holocene in age), overlying the Tosagua Formation (Oligocene – Miocene in age), made by two different members, the Villingota member, with white and grey limestones and with local intercalation of sandstones and the Dos Bocas member, made by coffee-colored lutites in layer thick from few centimeters to several decimeters, with local intercalation of silts and sands and dolomite lents. Such formations are related to the activity of the Rio Portoviejo, a river with direction SSE-NNW, which created the alluvial plain on which the city is founded.

III. DATA AND METHODS

In order to generate and thus interpret displacement maps, Sentinel-1 and COSMO-SkyMed SAR data were downloaded and processed. Sentinel-1 data are part of the European Copernicus program managed by ESA (European Space Agency) and are collected by satellites employed in a continuous Earth coverage, with the aim of creating an updated large global archive of the planet, freely available on the online Open Access Hub. They were acquired in both the two geometries

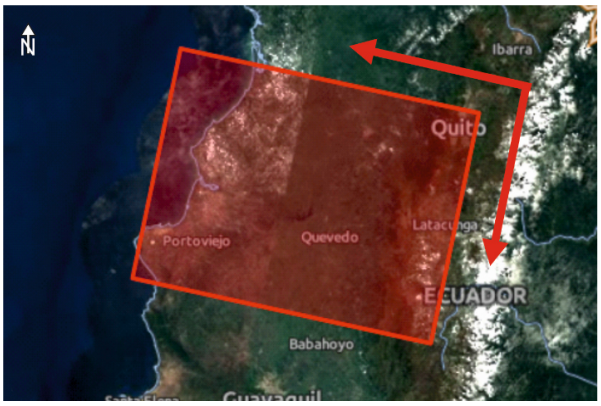

Figure 2: Ascending Sentinel-1 Frame

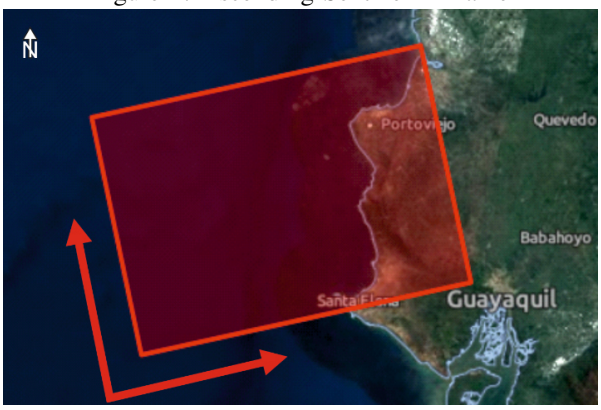

Figure 3: Descending Sentinel-1 Frame

of acquisition: descending (03/04/2016 and 27/04/2016) and ascending (03/04/2016 and 09/05/2016) (Fig. 2 and Fig. 3). The COSMO-SkyMed (Constellation of Small Satellites for Mediterranean basin Observation) is a 4-spacecraft constellation, conceived by ASI (Italian Spatial Agency), and funded by the Italian Ministry of Research (MIUR) and the Italian Ministry of Defense (MoD). The COSMO-SkyMed data have been gathered with the aim of observing the post-earthquake

deformations, covering the time interval between October 2016 and April 2017, for a total of 25 images acquired over the descending orbit.
The Differential SAR Interferometry has been implemented for such scenario to retrieve the land displacements from the interferometric phase once unnecessary contributions have been removed [18].

A. Interferometric phase

The interferometric phase variation can be split into different contributions:

- a contribution due to the terrain elevation, called **topographic phase**;
- a contribution due to the earth curvature, called **flat earth phase**;
- a contribution due to the presence of the **atmosphere**, called α;
- a contribution due to the **baseline** related to the different position of the satellite during the two acquisitions;
- a contribution due to the possible **land displacement**, Δr;
- a contribution due to the **noise** of the SAR system, the **reflectivity variation** of the target, the **SNR** and the **instrumental noise**.

The complete formulation is given by Equation (1):

$$\Delta\varphi = \frac{4\pi}{\lambda}\Delta r + \Delta_{topographic} + \Delta_{flat} + \alpha + t + noise \qquad (1)$$

B. Processing of COSMO-SkyMed data

COSMO-SkyMed data have been processed through the CPT technique developed by researchers of the UPC (Universitat Politècnica de Catalunya) in Barcelona [19]. The main steps of its processing are:

1) the generation of the best interferogram set among all the available images;
2) the selection of the pixels with reliable phase within the employed interferograms;
3) the phase analysis of the interferograms in order to calculate deformation time series of the period of observation.

The selection of the best set of interferograms is done selecting the temporal baseline, the spatial baseline and the Doppler frequency. The interferogram selection is then achieved using the Delaunay method for the triangulation of the available images. The pixel selection is achieved exploiting a coherence-based method, the coherence stability pixel selection criterion. In this framework, first a temporal averaging of all coherence maps is carried out, then a minimum threshold of coherence is fixed, and finally only the pixels presenting coherence values higher than the established threshold are selected for its later DInSAR processing. The coherence stability method works with multi-looked interferograms, making this approach more suited when working with distributed scatterers. In addition, it is important to highlight that this method provides accurate estimations even when a few number of interferograms is available

C. Processing of Sentinel-1 data

Sentinel-1 data have been processed through the open source Toolbox, available on the ESA website, and based on a common architecture framework, named SNAP, a collection of processing tools, and display and analysis applications able to calibrate, filter, coregistrate, orthorectify and thus generate the interferograms from the SAR images [20].

1) Interferogram formation: in order to perform the interferometric processing, two or more Single Look Complex (SLC) products of the same area, acquired from slightly different satellite position, are necessary. In Sentinel-1 IW (Interferometric Wide Swath) SLC products, three subswaths can be found (IW1, IW2, IW3). Each subswath corresponds to an adjacent acquisition through the TOPS (Terrain Observation by Progressive Scans) mode. Within a subswath, TOPS data are acquired in nine bursts separated by demarcation zones [21]. Before coregistrating the two images, it is necessary to use the *Split and Apply Orbit* operator, that allows to select the polarization and one of the three subswaths; furthermore this same operator applies the orbit correction. For interferometric processing, two or more images must be coregistered into a stack. The pixels in slave images will be moved to be aligned with the master image. Coregistration assures that each ground target contributes to the same pixel in both the master and the slave image. To perform the coregistration it is necessary to use the *Back-Geocoding* operator. The interferogram is formed by cross multiplying the master image with the complex conjugate of the slave, so the amplitude of both images is multiplied and the phase is obtained by subtracting the phase between the two images. The operator who generates the interferogram is the *Interferogram Formation*. In order to remove the demarcation zones it is necessary to use the operator *TOPSAR-Deburst*. Moreover, to decrease the computational effort it is possible to create a subset around the area of interest.

2) Generation of the displacement map: in order to estimate the displacements of the ground, the unnecessary phase contributions must be removed. If a digital elevation model (DEM) is available, the altitude contribution can be subtracted from the interferometric phase [22] applying the *Topographic phase removal* operator. To be able to unwrap the phase properly, the SNR must be increased by filtering the phase (note that where there is loss of coherence, the interference pattern is irredeemably lost). The *Goldstein Phase Filter* operator and the *Multilooking* operator are the most used for the phase filtering. It's important to observe that the interferogram provides an ambiguous measurement of relative terrain altitude due to the 2π cyclic nature of interferometric phase. The phase unwrapping is the process of recovering unambiguous phase data from a two dimensional array of phase values. The operation of phase unwrapping is carried out by the *SNAPHU* algorithm that is external to SNAP [23]. Note that the quality and reliability of the results depend mainly on the level of the relative coherence between the two input images. After importing the file processed with *SNAPHU* in *SNAP*, the displacement map can be generated using the *Phase to Displacement* operator. Because of the scene topographical variation and of the satellite sensor tilt, a terrain correction is often needed. The *Range Doppler terrain correction* operator, that implements the Range Doppler orthorectification method, geocodes SAR images (in this way the geometric representation of the image will be as close as possible to the real world).

IV. RESULTS

Sentinel-1 imagery has been acquired with a timespan of 24 days, as regards the descending dataset, to optimize the interferogram, having a better coherence. The general coherence has shown values of ca. 0.4, with, as expected, higher values in the urban area and along the main infrastructures, and lower values in the rural part, outside the city. As already above explained in detail, for the generation of the interferogram, the first operation is to eliminate the topographic phase, an operation which allows to eliminate the contribution of the phase related to the ground elevation, and this is achieved by using a Digital Elevation Model (DEM), automatically downloaded by the Sentinel-1 toolbox. Thus, the interferometric phase is filtrated through the Goldstein filter, reducing the residual fringes and improving the accuracy of the interferogram, and successively unwrapped to eliminate phase ambiguity and to produce the displacement map, for the ascending and the descending orbits. The maximum final displacement registered by the generated interferogram is about 50 cm (Figure 4), with the highest displacements located in the southern and western part of the city of Portoviejo. The effects of the earthquake and of the following ground displacements were strongly advisable on the structures and infrastructures. The damage report provided by EERI (Earthquake Engineering Research Institute) has been compared to the displacement map here generated. For instance, two examples of major failure in the Portoviejo area are the Rio Chico bridge and Mejia Bridge [24]. At the

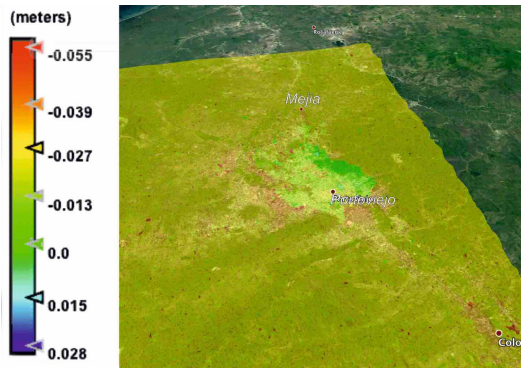

Figure 4: Displacement map from Sentinel-1 interferograms

Mejia bridge the embankments suffered of a general failure, as well as damage was mostly found on the south embankment, where the road level collapsed along a failure plane and due to a lateral displacement of the toe of the slope. DInSAR-derived observation clearly highlighted the displacement of the Mejia Bridge area, where a displacement pattern of ca. 50 cm is detected, covering the whole area (Figure 5 compared with the picture shown in Figure 6). Minor instability was found on the northern side of the infrastructure [24]. Also, steels buildings have suffered of minor damage, as the ECU911, the security service of Ecuador in Portoviejo, affecting mostly the masonry partitions, showing severe cracks. However, the interferogram highlighted a high displacement rate, up to 50 cm in the timespan considered (Fig. 7a). The Applied Sciences Faculty Building of Portoviejo's National University also suffered by diffuse damage, due to lack of attention to several important seismic details, as, for instance, captive columns, missing

Figure 5: Focus on the Mejia Bridge area

Figure 6: Failure of the Mejia Bridge (EERI, 2016)

confining reinforcement in columns and column-girder joints and inadequate stirrups (Fig. 7b). Besides the above-mentioned aspect, the displacement map highlight that the area suffers of severe deformation, of about 20 cm. Another witness of the displacement registered by SAR sensors in correspondence of damage surveyed by EERI team is the Mutualista Pichincha building, which originally had ten levels, and which after the earthquake had the floors from five to seven completely collapsed, causing the upper levels to lean toward the west. In this case displacements registered for pixels located in the area of the building have been of about 25 cm (Fig. 7c).

As regards the COSMO-SkyMed data, the first results of the CPT technique so far obtained show a full resolution image (Fig. 8 on the left) of the study area very clear, and a coherence map with mean coherence of 0.6, where the highest values are over the inhabited areas and the lowest values over the surrounding of the urban area (Fig. 8 on the right). Such products represent a first step for a complete analysis of the displacement occurring during the post-earthquake phase in Portoviejo, analysis that is still in progress. The displacement map related to the NE sector of the city of Portoviejo shows a deformation pattern which may have been triggered by the earthquake. Such pattern, considering the slope and the shape, may be attributed to a slow-shallow landslide, activated in the aftermath of the shakes (Fig.9a). In detail, the time series analysis highlighted a faster sector, along the main scarp of the landslide, with displacemnt of 0.8 cm in 7 months of analysis (from October 2016 to April 2017), as well as a slower behavior of the landslide is displayed along the toe of the landslide, with displacements of 0.35 mm in 7 months(Fig.9b).

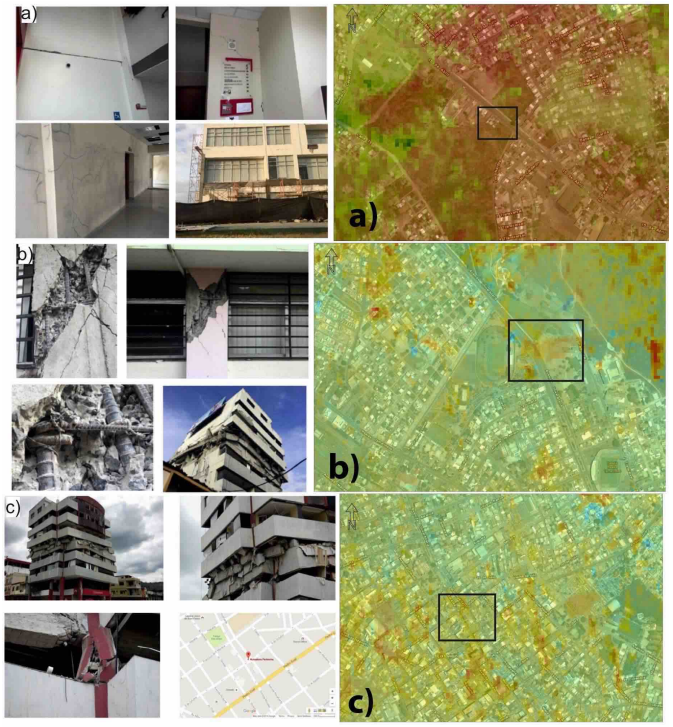

Figure 7: a) ECU911 damage reported by EERI on the left, Sentinel-1 displacement map on the right. The black square indicates the area of the ECU911 building; b) Applied Science Faculty Building of Portoviejo's National University damage reported by EEERI on the left, Sentinel-1 displacement map on the right. The black square indicates the area of the University building; c) Pichincha building damage reported by EEERI on the left, Sentinel-1 displacement map on the right. The black square indicates the area of the Pichinca building.

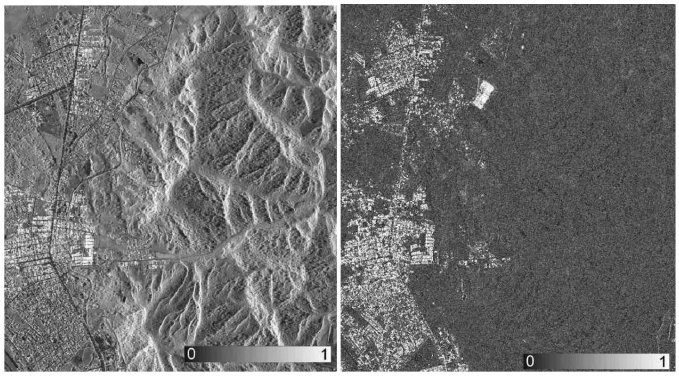

Figure 8: COSMO Coherence map: full resolution on the left; urban area on the right

It is worth to point out that such sector showed considerable displacements also in the Sentinel-1 analysis, related to the earthquake effects, thus demonstrating the activation of the landlside in correspondence of the shake. The COSMO-SkyMed analysis thus shows that the landslide has still an active state of activity in the months following the main phenomenon.

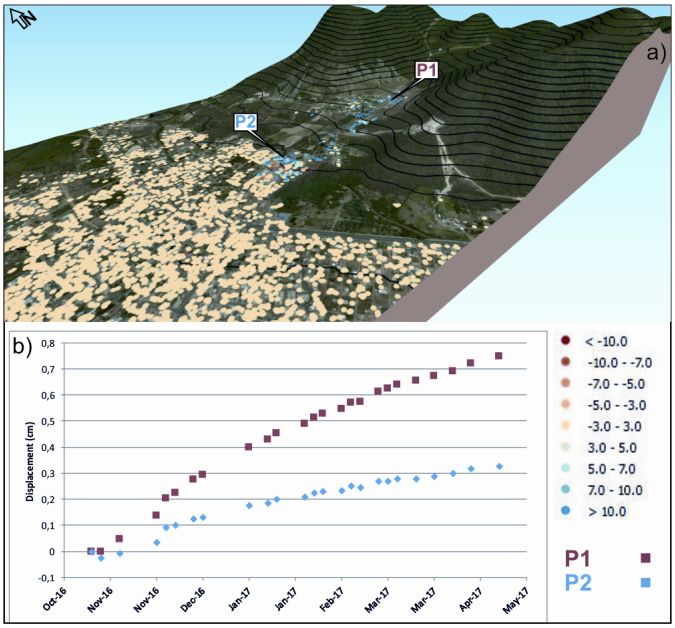

Figure 9: Displacement rate map of the NE sector of Portoviejo (a); Time-series analysis of the points P1 and P2 (b) (whose location is shown in (a))

V. CONCLUSIONS AND FUTURE DEVELOPMENTS

With this work the reliability of DInSAR as a tool for the detection and the monitoring of earthquake-induced displacements has been proved, as testified by the damage cases highlighted by the EERI team in the city of Portoviejo, Ecuador, hit by a 7.8 Mw earthquke on April 16, 2016. In particular, the role of remote sensing, thanks to the continuous acquisition and the short revisit time in the case of Sentinel-1, together with the good accuracy of the data, might be fundamental also for the monitoring and control of building and infrastructures behavior.

Moreover, the availability of open source software able to extract information from such imagery enhances a low-cost and easy continuous monitoring of areas at risk. As regards the study area, to enhance a prolonged monitoring of the effects of ground displacements on the inhabited areas, the post-earthquake phase will be accurately analyzed by the COSMO-SkyMed stack, which, characterized by a higher resolution and processed through the Coherent Pixel Technique, showed promising outcomes in a first phase. Indeed, such analysis, related to the NE sector of the city highlighted the activation of a landslide during and after the main shake. Therefore, the investigation over the whole area of Portoviejo will enable a complete definition of the deformations induced by the earthquake, both on the building area and on the sourronding environment. More extensive work is in progress.

REFERENCES

[1] L. Vranken, P. V. Turnhout, V. D. E. M, L. Vandekerchove, and J.Poesen, "Economic Valuation of Landslide Damage in Hilly Regions: A Case Study from Flanders, Belgium," *Science of the Total Environment*, vol. 447, pp. 323–336, 2013.

[2] G. . Lavecchia, R. Castaldo, R. Nardis, V. D. Novelli, F. Ferrarini, S. Pepe, F. Brozzetti, G. Solaro, D. Cirillo, M. Bonano, P. Boncio, F. Casu, C. D. Luca, R. Lanari, M. Manunta, M. Manzo, A. Pepe, I. Zinno, and P. Tizzani, "Ground Deformation and Source Seometry of the 24 August 2016 Amatrice Earthquake (Central Italy) Investigated Through Analytical and Numerical Modeling of DiNSAR Measurements and Structural-Geological Data," *Geophysical Research Letters*, vol. 43, no. 24, 2016.

[3] V. D. Novellis, S. Carlino, R. Castaldo, A. Tramelli, C. D. Luca, N. A. Pino, S. Pepe, V. Convertito, I. Zinno, P. D. Martino, M. Bonano, F. Giudicepietro, F. Casu, G. Macedonio, M. Manunta, C. Cardaci, M. Manzo, D. D. Bucci, G. Solaro, G. Zeni, R. Lanari, F. Bianco, and P. Tizzani, "The 21 August 2017 Ischia (Italy) Earthquake Source Model Inferred from Seismological, GPS, and DiNSAR Measurements," *Geophysical Research Letters*, 2018.

[4] S. Tessitore, A. Fernández-Merodo, G. Herrera, R. Tomás, M. Ramondini, M. Sanabria, J. Duro, J. Mulas, and D. Calcaterra, "Comparison of Water-level, Extensometric, DiNSAR and Simulation Data for Quantification of Subsidence in Murcia City (SE Spain)," *Hydrogeology journal*, vol. 24, no. 3, pp. 727–747, 2016.

[5] S. Fiaschi, S. Tessitore, R. Bonì, D. D. Martire, V. Achilli, S. Borgstrom, A. Ibrahim, M. Floris, C. Meisina, M. Ramondini, and D. Calcaterra, "From ERS-1/2 to Sentinel-1: Two Decades of Subsidence Monitored Through A-DiNSAR Techniques in the Ravenna Area (Italy)," *GIScience & Remote Sensing*, vol. 54, no. 3, 2017.

[6] P. Confuorto, D. D. Martire, G. Centolanza, R. Iglesias, J. Mallorqui, A. Novellino, S.Plank, M. Ramondini, K. Thuro, and D. Calcaterra, "Post-Failure Evolution Analysis of a Rainfall-Triggered Landslide by Multi-Temporal Interferometry SAR Approaches Integrated with Geotechnical Analysis," *Remote sensing of environment*, vol. 188, pp. 51–72, 2017.

[7] D. D. Martire, M. Paci, P. Confuorto, S. Costabile, F. Guastaferro, A. Verta, and D. Calcaterra, "A Nation-Wide System for Landslide Mapping and Risk Management in Italy: The Second Not-Ordinary Plan of Environmental Remote Sensing," *International Journal of Applied Earth Observation and Geoinformation*, vol. 63, pp. 143–157, 2017.

[8] O. Mora, J. J. Mallorqui, and A. Broquetas, "Linear and Nonlinear Terrain Deformation Maps from a Reduced Set of Interferometric SAR Images," *IEEE Transactions on Geoscience and Remote Sensing*, vol. 41, no. 10, pp. 2243–2253, 2003.

[9] USGS, "M7.8 - 29km sse of Muisne, Ecuador," *Bulletin of the Seismological Society of America*, vol. 82, no. 2, pp. 1018–1040, 2016.

[10] I. G. E. P. Nacional, "Actualizacion de las Replica," *Informe Sismico Especial*, no. 25, 2016.

[11] J. R. Orellana, "Continuan las Replicas del Sismo de Pedernales," *Informe Sismico Especial*, no. 14, 2016.

[12] G. P. Hayes, D. J. Wald, and R. L. Johnson, "Slab1. 0: A Three-dimensional Model of Global Subduction Zone geometries," *Journal of Geophysical Research: Solid Earth*, vol. 117, no. B1, 2012.

[13] H. Parra, M. B. Benito, and J. M. Gaspar-Escribano, "Seismic Hazard Assessment in Continental Ecuador," *Bulletin of Earthquake Engineering*, vol. 14, no. 8, pp. 2129–2159, 2016.

[14] R. Trenkamp, J. N. Kellogg, J. T. Freymueller, and H. P. Mora, "Wide Plate Margin Deformation, Southern Central America and Northwestern South America, CASA GPS Observations," *Journal of South American Earth Sciences*, vol. 15, no. 2, pp. 157–171, 2002.

[15] F. Michaud, C. Witt, and J. Y. Royer, "Influence of the Subduction of the Carnegie Volcanic Ridge on Ecuadorian Geology: Reality and Fiction," *Backbone of the Americas: Shallow Subduction, Plateau Uplift, and Ridge and Terrane Collision*, vol. 204, p. 217, 2009.

[16] G. Franco, H. Stone, B. Ahmed, S. Chian, F. Hughes, N. Jirouskova, S. Kaminski, J. Lopez, N. van Drunen, and Q. M, "The April 16 2016 Mw7. 8 Muisne Earthquake in Ecuador–Preliminary Observations from the EEFIT Reconnaissance Mission of May 24-June 7," *Journal of South American Earth Sciences*, 2017.

[17] M. F. Gallegos and G. R. Saragoni, "Analysis of Strong-Motion Accelerograph Records of the 16 April 2016 Mw 7.8 Muisne, Ecuador Earthquake," 2017.

[18] U. Wegmuller, C. Werner, and T. Strozzi, "SAR interferometric and differential interferometric processing chain," 1998.

[19] R. Iglesias, J. J. Mallorqui, D.Monells, C. López-Martínez, X. Fabregas, A. Aguasca, J. A. Gili, and J. Corominas, " PSI Deformation Map Retrieval by means of Temporal Sublook Coherence on Reduced Sets of SAR Images," *Remote Sensing*, vol. 7, no. 1, pp. 530–563, 2015.

[20] L. Veci, P. Prats-Iraola, and C. F. F. N. . E. M. R. Scheiber, R., "The Sentinel-1 Toolbox," pp. 1–3, 2014.

[21] L. Veci, "Sentinel1- Toolbox: TOPS Interferometry Tutorial," https://sentinel.esa.int/web/sentinel/toolboxes/sentinel-1/tutorials, August 2016.

[22] A. Ferretti, A. Monti-Guarnieri, C. Prati, F. Rocca, and D. Massonet, "InSAR principles-guidelines for SAR interferometry processing and interpretation," 2007.

[23] C. Chen and H. Z. S. University), "Snaphu website," http://web.stanford.edu/group/radar/softwareandlinks/sw/snaphu/.

[24] E. E. R. Institute, "EERI Earthquake Reconnaissance Team Report: M7.8 Muisne, Ecuador Earthquake on April 16, 2016," 2014.

[25] L. Veci, " Sentinel1- Toolbox: Interferometry Tutorial," https://sentinel.esa.int/web/sentinel/toolboxes/sentinel-1/tutorials, March 2016.